Characterisation of the neonatal brain using myelin-sensitive magnetisation transfer imaging

Manuel Blesa Cábez [a,1,*], Kadi Vaher[a,*], Elizabeth N. York[b,c,d], Paola Galdi[a], Gemma Sullivan[a], David Q. Stoye[a], Jill Hall[a], Amy E. Corrigan[e], Alan J. Quigley[e], Adam D. Waldman[b,d], Mark E. Bastin[b,d], Michael J. Thrippleton[b,d], James P. Boardman[a,b]

Author affiliations

[a]MRC Centre for Reproductive Health, University of Edinburgh, Edinburgh, EH16 4TJ, UK

[b]Centre for Clinical Brain Sciences, University of Edinburgh, Edinburgh, EH16 4SB, UK

[c]Anne Rowling Regenerative Neurology Clinic, Edinburgh, EH16 4SB, UK

[d]Edinburgh Imaging, University of Edinburgh, Edinburgh, UK

[e]Royal Hospital for Children & Young People, Edinburgh, EH16 4TJ, UK

[1]Corresponding author: Manuel Blesa Cábez, Queen's Medical Research Institute, 47 Little France Crescent, Edinburgh EH16 4TJ, UK. Email: manuel.blesa@ed.ac.uk

*These authors contributed equally to the work.

Abstract

A cardinal feature of the encephalopathy of prematurity is injury/dysmaturation of developing white matter and subsequent hypomyelination. Magnetisation transfer imaging (MTI) offers surrogate markers for myelination including magnetisation transfer ratio (MTR) and magnetisation transfer saturation (MTsat). In this work, using data from 105 neonates, we use MTR, MTsat and approximation of R1 (R1app) to characterise myelination in the developing brain by investigating how these measures are affected by gestational age at scan and preterm birth. We explore correlations of the three measures with fractional anisotropy (FA) and T1w/T2w ratio which are commonly used markers of white matter integrity in development. We used two complementary analysis methods: voxel-wise analysis across the white matter skeleton, and tract-of-interest analysis across 16 major white matter tracts. We found that MTR, MTsat and R1app positively correlate with gestational age at scan. Preterm infants at term-equivalent age had lower values of R1app across the brain and MTsat in the genu and splenium of the corpus callosum, while MTR was higher in central white matter regions, the cortico-spinal tract and the uncinate fasciculus. Correlations of MTI metrics with FA and T1w/T2w ratio revealed that there were moderate positive correlations between T1w/T2w and MTsat and MTR at voxel-level, but at tract-level FA had stronger positive correlations with these metrics. This work demonstrates that MTI captures features consistent with lower myelination and cellular/axonal density in preterm infants at term-equivalent age compared to term controls. Furthermore, correlations between MTI-derived features and conventional measures from dMRI could provide new understanding about the contribution of myelination to non-specific imaging metrics used to characterise early brain development.

Keywords: magnetisation transfer, preterm birth, neonate, white matter, myelin

Abbreviations

AF	arcuate fasciculus
ATR	anterior thalamic radiation
CC genu	corpus callosum genu/forceps minor
CC splenium	corpus callosum splenium/forceps major
CCG	cingulum cingulate gyrus
CST	corticospinal tract
dHCP	developing human connectome project
dMRI	diffusion magnetic resonance imaging
FA	fractional anisotropy
FDR	false discovery rate
FWER	family-wise error correction
GA	gestational age
GM	grey matter
IFOF	inferior fronto-occipital fasciculus
ILF	inferior longitudinal fasciculus
MRI	magnetic resonance imaging
MTI	magnetisation transfer imaging
MTR	magnetisation transfer ratio
MTsat	magnetisation transfer saturation
R1app	approximation of R1
ROI	region of interest
SNR	signal-to-noise ratio
TE	echo time
TEA	term-equivalent age
TFCE	threshold-free cluster enhancement
TR	repetition time
UNC	uncinate fasciculus
WM	white matter

Highlights

- We applied magnetisation transfer imaging (MTI) in the neonatal brain
- MTR, MTsat and R1app positively correlate with gestational age at scan
- Preterm birth associated with lower values of R1app and MTsat, and higher MTR
- Correlations between MTI and other white matter integrity metrics were explored
- MTI captures myelin progression and suggests lower myelination in the preterm brain

1 Introduction

The integrity of brain development during pregnancy and the new born period is critical for life-long cognitive function and brain health. During the second and third trimesters of pregnancy, there is a phase of rapid brain maturation characterised by volumetric growth, increases in cortical complexity, white matter (WM) organisation and myelination (Counsell et al., 2019; Dubois et al., 2021). Early exposure to extrauterine life due to preterm birth, defined as birth < 37 weeks of gestation, affects around 11% of births and is closely associated with neurodevelopmental, cognitive and psychiatric impairment (Johnson and Marlow, 2017; Nosarti et al., 2012; Wolke et al., 2019), and alterations to brain development that are apparent using magnetic resonance imaging (MRI) techniques (Boardman and Counsell, 2019; Counsell et al., 2019; Pecheva et al., 2018).

MRI allows characterisation of the neonatal brain *in vivo*. There are several MRI techniques that provide different and complementary information about tissue microstructure and properties. Structural MRI (T1- and T2-weighted) and diffusion MRI (dMRI) have revealed an MRI phenotype of preterm birth that includes reductions in global and regional tissue volume, and altered microstructural integrity of the WM (Counsell et al., 2019; Pecheva et al., 2018). However, whilst these modalities are influenced by microstructural properties of the underlying tissue including axonal density and diameter, myelination and water content, they are not specific to myelin (Mancini et al., 2020; van der Weijden et al., 2020). The T1w/T2w ratio has been used as a proxy measure for myelination (Glasser and van Essen, 2011; Soun et al., 2017; Thompson et al., 2022); however, the degree to which it is sensitive to myelin has been contested (Arshad et al., 2017; Uddin et al., 2018).

Pre-oligodendrocytes are particularly vulnerable to hypoxia-ischaemia and inflammation associated with preterm birth (Back and Volpe, 2018; Volpe et al., 2011). Although this cell population is mostly replenished following primary injury, subsequent differentiation into myelin-producing oligodendrocytes can fail, leading to hypomyelination (Billiards et al., 2008; Volpe, 2019). Therefore, imaging tools that more specifically model myelination in early life could enhance biology-informed assessment of preterm brain dysmaturation.

Magnetisation transfer imaging (MTI) is a family of MRI techniques sensitive to subtle pathological changes in tissue microstructure which cannot typically be quantified with conventional MRI (Sled, 2018). MTI is based on the exchange of magnetisation between immobile protons associated with macromolecules, and mobile protons in free water. MTI is sensitive to myelin-associated macromolecules such as cholesterol, myelin basic protein, sphingomyelin and galactocerebrides, and thus it provides a surrogate marker of myelin integrity (Mancini et al., 2020). To date, MTI has mainly been used to study WM diseases such as multiple sclerosis (Sled, 2018; York et al., 2022b).

Magnetisation transfer ratio (MTR), calculated as the percentage change in signal with and without off-resonance radiofrequency saturation, is the most widely used MTI metric. MTR

is, however, susceptible to transmit ($B1^+$) field inhomogeneities (Helms et al., 2010a) and T1 relaxation effects, and varies widely depending upon specific acquisition parameters (Samson et al., 2006; York et al., 2022c). Biological interpretation of MTR is therefore challenging, which presents a barrier to clinical translation. The addition of a T1w sequence allows computation of magnetisation transfer saturation (MTsat) which inherently corrects for $B1^+$ inhomogeneities and T1 relaxation to a substantial degree (Helms et al., 2008b; Samson et al., 2006). MTsat hence addresses some limitations of MTR within clinically feasible acquisition times and the resulting parametric maps have visibly better tissue contrast compared with MTR (Helms et al., 2008b; Samson et al., 2006; York et al., 2022b). Higher values of MTR and MTsat are associated with greater myelin density.

In neonates, MTR has been used to characterize brain development during the preterm period from birth up to term-equivalent age (TEA): in general, MTR values in WM increase with gestational age (GA) at scan (Nossin-Manor et al., 2015, 2013, 2012; Zheng et al., 2016). In addition, at the age of 4 years, MTR correlates with cognitive outcomes in children who were born preterm (Vandewouw et al., 2019). R1 mapping has been used to show that, during early infancy, myelin content at birth and spatial gradients of myelin development together explain the rate of myelin growth across the WM of the human brain (Grotheer et al., 2022). To the best of our knowledge, MTsat has not previously been applied in the human neonatal brain.

In this work, we aimed to obtain a more specific description of brain myelination processes by applying MTI in the neonatal period. We had three objectives: 1) to characterise the associations of MTsat, MTR and R1app (approximation of R1) in neonatal WM with GA at MRI scan; 2) to test the hypothesis that one or more myelin-sensitive features would differ between preterm infants at TEA and term controls; and 3) to assess the relationship between MTI metrics and the T1w/T2w ratio, a commonly used myelin proxy, and fractional anisotropy (FA), which is most robustly associated with encephalopathy of prematurity but is not specific to myelination.

2 Material and methods

2.1 Participants and data acquisition

Participants were very and extremely preterm infants (GA at birth < 32 completed weeks) and term-born controls recruited as part of a longitudinal study designed to investigate the effects of preterm birth on brain structure and long-term outcome (Boardman et al., 2020). The cohort exclusion criteria were major congenital malformations, chromosomal abnormalities, congenital infection, overt parenchymal lesions (cystic periventricular leukomalacia, haemorrhagic parenchymal infarction) or post-haemorrhagic ventricular dilatation. The study was conducted according to the principles of the Declaration of Helsinki, and ethical approval was obtained from the UK National Research Ethics Service. Parents provided written informed consent. 105 neonates (83 preterm and 22 term) who

underwent MTI at TEA at the Edinburgh Imaging Facility (Royal Infirmary of Edinburgh, University of Edinburgh, UK) were included in the current study.

A Siemens MAGNETOM Prisma 3 T clinical MRI system (Siemens Healthcare Erlangen, Germany) and 16-channel phased-array paediatric head coil were used to acquire a three-dimensional (3D) T1w magnetisation prepared rapid gradient echo (MPRAGE) structural image (voxel size = 1 mm isotropic, echo time [TE] = 4.69 ms and repetition time [TR] = 1970 ms); 3D T2-weighted SPACE images (T2w) (voxel size = 1mm isotropic, TE = 409 ms and TR = 3200 ms) and axial dMRI data. dMRI volumes were acquired in two separate acquisitions to reduce the time needed to re-acquire any data lost to motion artifacts: the first acquisition consisted of 8 baseline volumes (b = 0 s/mm^2 [b0]) and 64 volumes with b = 750 s/mm^2; the second consisted of 8 b0, 3 volumes with b = 200 s/mm^2, 6 volumes with b = 500 s/mm^2 and 64 volumes with b = 2500 s/mm^2. An optimal angular coverage for the sampling scheme was applied (Caruyer et al., 2013). In addition, an acquisition of 3 b0 volumes with an inverse phase encoding direction was performed. All dMRI volumes were acquired using single-shot spin-echo echo planar imaging (EPI) with 2-fold simultaneous multi-slice and 2-fold in-plane parallel imaging acceleration and 2 mm isotropic voxels; all three diffusion acquisitions had the same parameters (TR/TE 3400/78.0 ms). Acquisitions affected by motion artifacts were re-acquired multiple times as required; dMRI acquisitions were repeated if signal loss was seen in 3 or more volumes. MTI consisted of three sagittal 3D multi-echo spoiled gradient echo images (TE = 1.54/4.55/8.56 ms, 2 mm isotropic acquired resolution): magnetisation transfer (TR = 75 ms, flip angle = 5°, gaussian MT pulse (offset 1200 Hz, duration 9.984 ms, flip angle = 500°) [MT_{on}]), proton density-weighted (TR = 75 ms, flip angle = 5° [MT_{off}]) and T1w (TR = 15 ms, flip angle = 14° [MT_{T1w}]) acquisitions. All acquisition parameters are detailed in the cohort protocol (Boardman et al., 2020).

Infants were fed and wrapped and allowed to sleep naturally in the scanner. Pulse oximetry, electrocardiography and temperature were monitored. Flexible earplugs and neonatal earmuffs (MiniMuffs, Natus) were used for acoustic protection. All scans were supervised by a doctor or nurse trained in neonatal resuscitation.

2.2 Data preprocessing

The image analysis was performed with MRtrix3 (Tournier et al., 2019), FSL 5.0.11 (Smith et al., 2004), ANTs (Avants et al., 2008), the developing Human Connectome Project (dHCP) pipeline (Makropoulos et al., 2018) and MATLAB R2022a.

dMRI processing was performed as follows: for each subject, the two dMRI acquisitions were first concatenated and then denoised using a Marchenko-Pastur-PCA-based algorithm (Veraart et al., 2016); eddy current, head movement and EPI geometric distortions were corrected using outlier replacement and slice-to-volume registration (Andersson et al., 2017, 2016, 2003; Andersson and Sotiropoulos, 2016); bias field inhomogeneity correction was performed by calculating the bias field of the mean b0 volume and applying the correction

to all the volumes (Tustison et al., 2010). The b = 750 s/mm^2 shell was used to calculate the FA maps.

Structural MRI (T1w and T2w) images were processed using the dHCP minimal processing pipeline to obtain the bias field corrected and coregistered T2w and T1w, brain masks, tissue segmentation and the different tissue probability maps (Makropoulos et al., 2018, 2014). T1w/T2w ratio maps obtained from this pipeline were edited to remove voxels with intensities higher than the mean + 5 standard deviations.

2.3 Magnetisation transfer imaging processing

MTI data were processed as previously described (York et al., 2022b, 2020). The three echoes were summed together to increase the signal-to-noise ratio (SNR) (Helms and Hagberg, 2009) for each MT image (MT_{off}, MT_{on} and MT_{T1w}). MT_{on} and MT_{T1w} images were coregistered to the MT_{off} image. From (Helms et al., 2010b, 2008a) we can define the amplitude of the spoiled gradient echo at the echo time (App) as:

$$Aapp = \frac{S_{T1w} * (S_{off} * TR_{T1w} * \alpha_{off}^2 - S_{off} * TR_{off} * \alpha_{T1w}^2)}{\alpha_{off} * \alpha_{T1w} * (S_{off} * TR_{T1w} * \alpha_{off} - S_{T1w} * TR_{off} * \alpha_{T1w})}$$

where *S*, *TR* and α represent the signal intensity the repetition time (in seconds) and the flip angle (in radians), respectively. The subscript *off* stands for the proton density-weighted acquisition and the subscript *T1w* for T1-weighted image.

The R1app is expressed as:

$$R1app = \frac{-\alpha_{off} * \alpha_{T1w} * (S_{off} * TR_{T1w} * \alpha_{off} - S_{T1w} * TR_{off} * \alpha_{T1w})}{2 * TR_{T1w} * TR_{off} * (S_{off} * \alpha_{T1w} - S_{T1w} * \alpha_{off})}$$

By combining R1app and Aapp, we can obtain the MTsat:

$$MTsat = \frac{-\alpha_{off}^2}{2} + \frac{(Aapp * R1app * TR_{off} * \alpha_{off})}{S_{on}} - R1app * TR_{off}$$

where S_{on} represents the intensity signal of the magnetization transfer weighted image.

Finally, the MTR can be obtained as follows:

$$MTR = 100 * \frac{S_{off} - S_{on}}{S_{off}}$$

2.4 Registration to a common space

MTsat, MTR and R1app maps were registered to the structural T1w (MPRAGE) images processed with the dHCP pipeline using ANTs symmetric normalisation (SyN) (Avants et al., 2008). The tissue probability maps for the grey matter (GM) and WM were obtained from the dHCP pipeline (Makropoulos et al., 2018). Nonlinear diffeomorphic multimodal registration was then performed between age-matched T2w and GM/WM tissue probability maps from the dHCP extended volumetric atlas (Fitzgibbon et al., 2020; Schuh et al., 2018)

to the subjects T2w and GM/WM tissue probability using SyN (Avants et al., 2008). This was combined with the corresponding template-to-template transformation to yield a structural-to-template (40 weeks GA) transformation, which was finally combined with the MTsat-to-structural transformation to obtain the final MTsat-to-template alignment.

2.5 Tract-based spatial statistics

The mean b0 EPI volume of each subject was co-registered to their structural T2w volume using boundary-based registration (Greve and Fischl, 2009). This was combined with the structural-to-template transformation to create the diffusion-to-template transformation and propagate the FA maps to the template space.

The FA maps were averaged and used to create the skeleton mask. MTsat, MTR and R1app parametric maps were propagated to template space using the MTsat-to-template transformation and projected onto the skeleton (Smith et al., 2006).

2.6 White matter tracts of interest

Sixteen WM tracts were generated in each subject's diffusion space as previously described (Vaher et al., 2022). Briefly, the tract masks were propagated from the ENA50 atlas (Blesa et al., 2020). These masks were used as a set of regions of interest (ROI) for seeding the tractography, creating the tracts in native diffusion space. Then, the tracts were binarised and propagated to MTsat space by combining the MTsat-to-structural and diffusion-to-structural transformations to calculate the mean values in each tract.

2.7 Statistical analysis

Tract-based statistical analyses were conducted in R (version 4.0.5) (R Core Team, 2022). We performed multivariate multiple linear regression analyses for all WM tracts, with the tract-average metric as the outcome and preterm status and GA at scan as the predictor variables. The outcome variables as well as GA at scan were scaled (z-transformed) before fitting the models, thus, the regression coefficients reported are in the units of standard deviations. P-values were adjusted for the false discovery rate (FDR) using the Benjamini-Hochberg procedure (Benjamini and Hochberg, 1995) across all MRI metrics separately for the effects of preterm birth and GA at scan. The WM tract results were visualised using ParaView (ParaView Developers, 2020), with standardised betas represented as the effect size.

Voxel-wise statistical analysis was performed using a general linear univariate model with PALM (Winkler et al., 2014). Two different contrasts were tested: correlation with GA at scan adjusting for prematurity, and term vs preterm comparison adjusting for GA at scan. Family-wise error correction (FWER) and threshold-free cluster enhancement (TFCE) were applied with a significance level of $p<0.05$ (Smith and Nichols, 2009).

The distributions of MTI metrics, FA and T1w/T2w ratio were compared using two-dimensional histograms of co-registered indexed voxels (RNifti and ggplot2::geom_bin2d

packages in R) (York et al., 2022a) and voxel-wise correlation analyses between the metrics were performed with repeated measures correlation as implemented in the R package *rmcorr* (Bakdash and Marusich, 2017); this was performed in the WM tissue segmentation obtained from the dHCP pipeline (Makropoulos et al., 2018). Tract-wise correlation coefficients were calculated using Pearson's r. The average Pearson's correlation coefficient across all tracts was calculated by first transforming the Pearson's r values to Fisher's Z, taking the average, and then back-transforming the value to Pearson's correlation coefficient (Corey et al., 1998).

2.8 Data and code availability

Requests for anonymised data will be considered under the study's Data Access and Collaboration policy and governance process (https://www.tebc.ed.ac.uk/2019/12/data-access-and-collaboration/). The scripts for the data analysis in this paper are available here: https://git.ecdf.ed.ac.uk/jbrl/neonatal-mtsat.

3 Results

3.1 Sample characteristics

The study group consisted of 105 neonates: 83 participants were preterm and 22 were term-born controls. Participant characteristics are provided in Table 1. Among the preterm infants, 15 (18.1%) had bronchopulmonary dysplasia (defined as need for supplementary oxygen ≥ 36 weeks GA), 3 (3.6%) developed necrotising enterocolitis requiring medical or surgical treatment, 15 (18.1%) had one or more episodes of postnatal sepsis (defined as detection of a bacterial pathogen from blood culture, or physician decision to treat with antibiotics for ≥ 5 days in the context of growth of coagulase negative *Staphylococcus* from blood or a negative culture but raised inflammatory markers in blood), and 2 (2.4%) required treatment for retinopathy of prematurity.

Table 1: Neonatal participant characteristics. The last column reports the p-values of the group differences computed with Student's t-test for continuous variables and Fisher's exact test for categorical variables. GA = gestational age; M/F = male/female.

	term (n=22)	**preterm (n=83)**	**p-value**
GA at birth (weeks)	39.57 (36.42 - 41.56)	29.48 (24.14 - 32.84)	n/a
Birth weight (grams)	3340 (2410 - 4295)	1334 (594 - 2380)	n/a
Birth weight z-score	0.167 (-2.295 - 1.970)	0.060 (-3.132 - 2.141)	0.632
GA at scan (weeks)	41.93 (40.00 - 46.14)	40.77 (37.84 - 45.84)	<0.001
M:F ratio	13:9	49:34	1

3.2 Magnetisation transfer imaging metrics in association with gestational age at scan and preterm birth

The average MTsat, MTR and R1app maps for the term and preterm infants are shown in Figure 1A. From visual inspection of the averaged maps, the most striking differences between the term and preterm groups is in R1app, where term infants have higher values across the brain. In comparison, MTsat and MTR show more similar values across the two groups, although preterm infants have lower MTsat values mostly in the frontal regions and higher MTR values in the central regions. Tract-averaged values for MTsat, MTR and R1app for term and preterm groups are provided in Supplementary Table 1 and visualised in Figure 1B. The highest MTsat and R1app values are observed in the corticospinal tract, whilst MTR is highest in the anterior thalamic radiation and cingulum cingulate, followed by the corticospinal tract. The lowest values for all three MTI metrics are observed in the inferior longitudinal fasciculus.

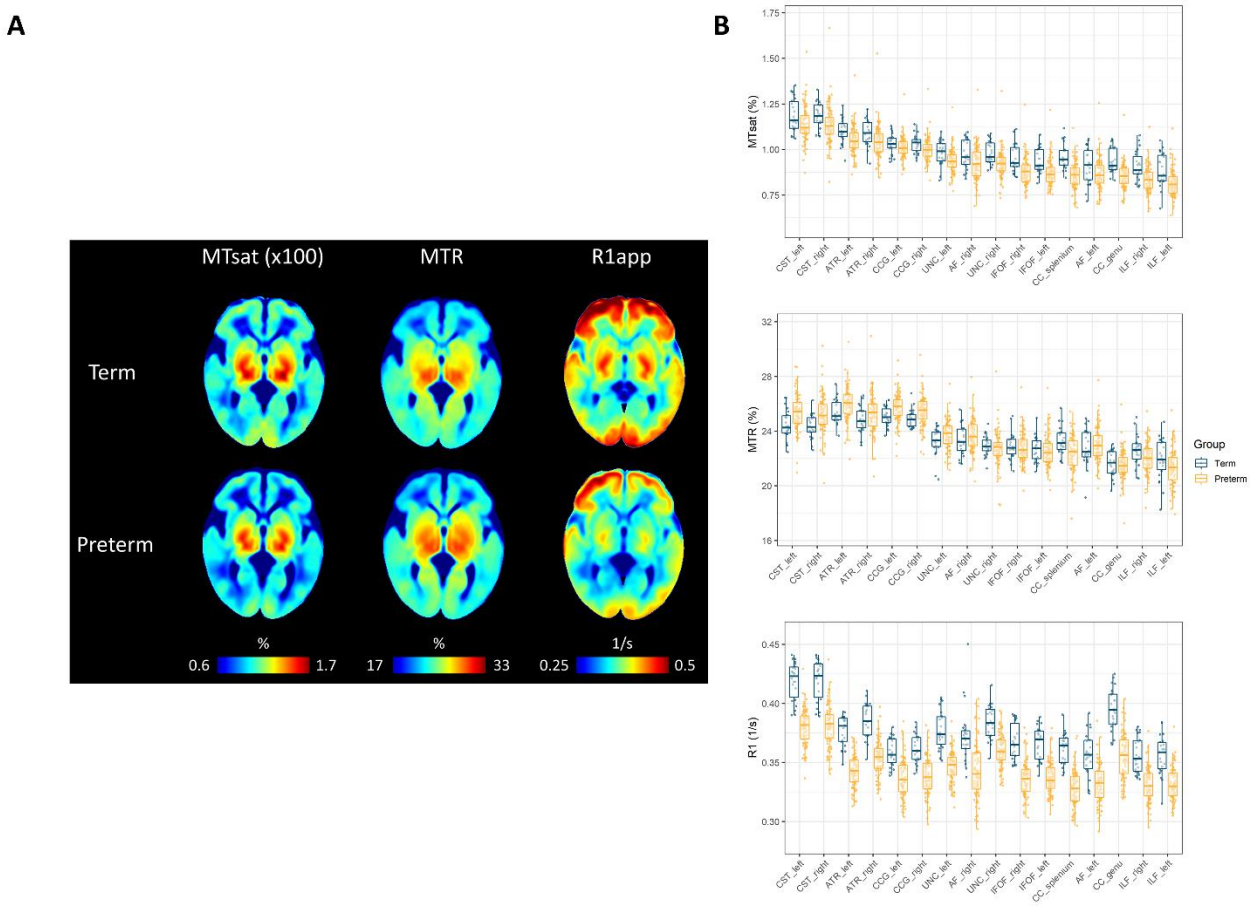

Figure 1: (A) Neonatal MTsat, MTR and R1app maps averaged across term and preterm subjects in the study. (B) Tract-averaged MTI metrics in the 16 white matter tracts; tracts are ordered by the values of MTsat. MTR = magnetisation transfer ratio, MTsat = magnetisation transfer saturation, R1app = approximation of longitudinal relaxation rate, CC genu = corpus callosum genu/forceps minor, CC splenium = corpus callosum splenium/forceps major, CST = corticospinal tract, IFOF = inferior fronto-occipital fasciculus, ILF = inferior longitudinal fasciculus, AF = arcuate fasciculus, UNC = uncinate fasciculus, CCG = cingulum cingulate gyrus, ATR = anterior thalamic radiation.

We took two complementary approaches to study the effect of GA at scan and preterm birth on the MTI metrics: voxel-wise in the WM skeleton, and ROI-based using mean values in 16 major WM tracts (Vaher et al., 2022).

In the neonatal period between 37-46 weeks of gestation, after adjusting for preterm birth, both MTsat and MTR are positively correlated with GA at scan in the WM. These results were visible on both voxel-wise (Figure 2) and tract-based analyses (Figure 3 left panel). The effect of GA at scan was less widely distributed (Figure 2) and with smaller effect sizes (Figure 3 left panel) for R1app.

The strongest effect of preterm birth can be observed in R1app: term infants have significantly higher values throughout the WM compared to the preterm group (Figure 3 right panels and Figure 4). Although we observed that both MTsat and MTR positively

correlate with GA at scan, the effect of preterm birth was different for these two metrics. MTsat did not show any statistically significant differences between term and preterm at the voxel level, except for a small cluster in the left frontal lobe (Figure 4). Some tracts had significantly higher values of MTsat in term compared to preterm infants, particularly the genu and splenium of the corpus callosum (Figure 3 right panel). In contrast, MTR was higher in preterm infants, particularly in the central WM regions, and in the cortico-spinal tract and uncinate fasciculus (Figure 3 right panel and Figure 4).

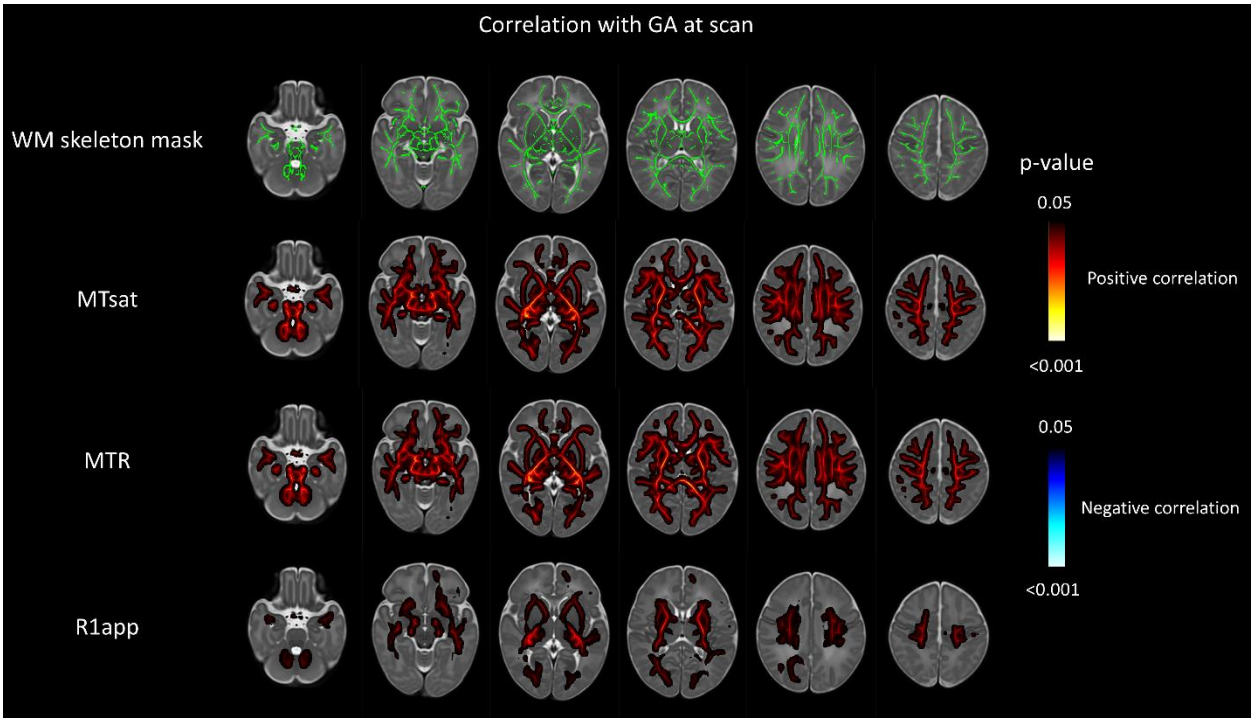

Figure 2: Voxel-wise analysis showing effects of GA at scan on magnetisation transfer imaging metrics when adjusting for preterm status. The first row represents the WM skeleton mask (green) where voxel values were compared. Voxels that have positive correlation with GA at scan are indicated in red-yellow; voxels that have negative correlations with GA at scan are indicated in blue-light blue, overlaid on the dHCP T2w 40 week template. Results are reported after 5000 permutations, p-values corrected using TFCE and FWE with a significance level of p<0.05. For visualisation: anatomic left is on the right side of the image. GA = gestational age; MTR = magnetisation transfer ratio, MTsat = magnetisation transfer saturation, R1app = approximation of longitudinal relaxation rate, TFCE = family-wise error correction, FWE = threshold-free cluster enhancement.

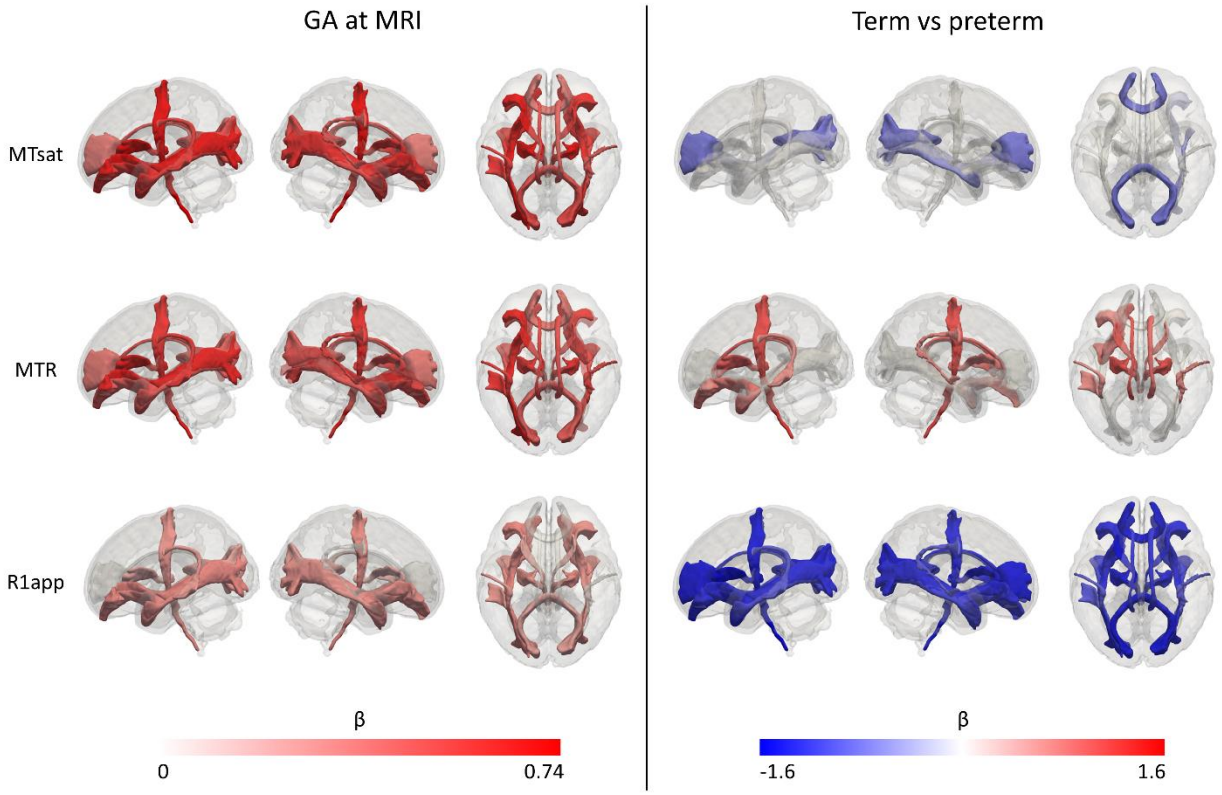

Figure 3: Results of the white matter tract-based analysis of magnetisation transfer imaging metrics at term-equivalent age showing the effects of GA at MRI (left panel) and differences in preterm infants versus term-born controls (right panel). Effect sizes are represented as standardised beta coefficients from the multiple regression where white matter tract values were the outcomes and preterm status and GA at scan the predictors; only statistically significant tracts (FDR-corrected across the three modalities) are coloured. Colour map for the effect sizes was calculated separately for the effects of preterm birth and GA at scan. In left panel, red indicates positive correlation with GA at MRI. In right panel, blue indicates higher values in term infants and red indicates higher values in preterm infants. GA = gestational age, MTR = magnetisation transfer ratio, MTsat = magnetisation transfer saturation, R1app = approximation of longitudinal relaxation rate.

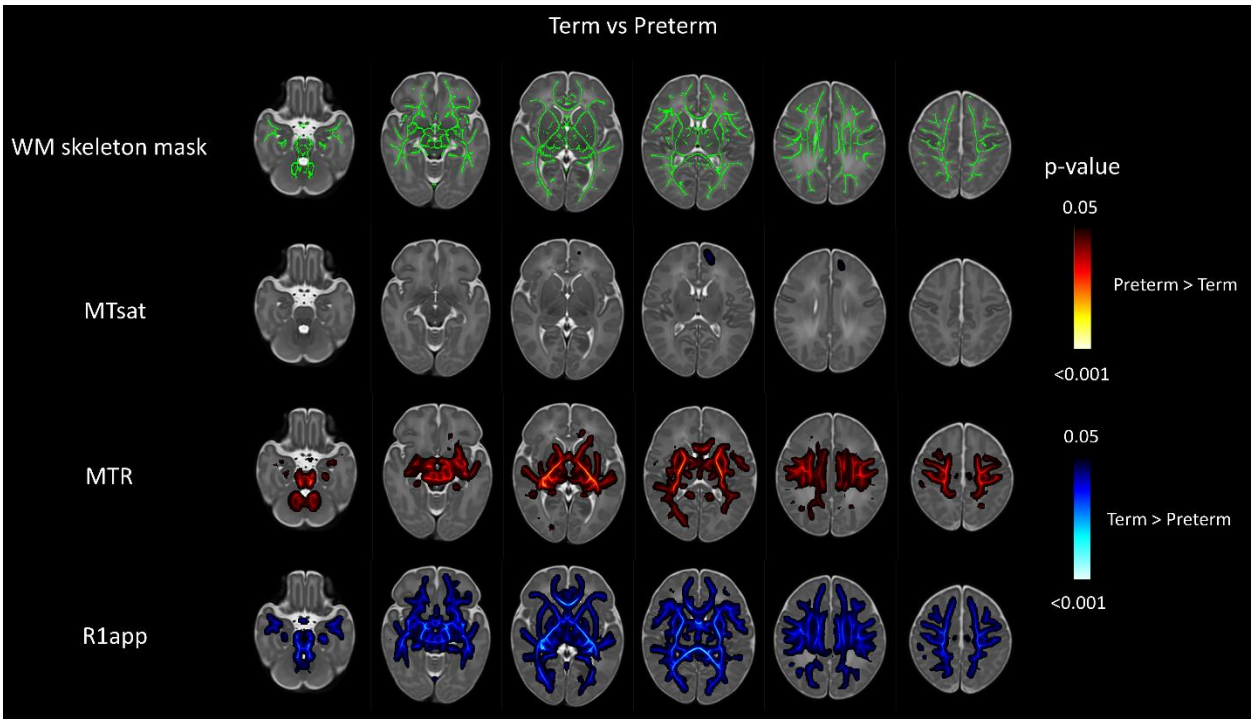

Figure 4: Voxel-wise analysis showing differences in magnetisation transfer imaging metrics in preterm infants at term-equivalent age versus term-born controls when adjusting for GA at scan. The first row represents the WM skeleton mask (green) where voxel values were compared. Voxels that have higher values in the preterm group compared with the term group are indicated in red-yellow; voxels that have higher values in term group compared with preterm group are indicated in blue-light blue, overlaid on the dHCP T2w 40 week template. Results are reported after 5000 permutations, p-values corrected using TFCE and FWE with a significance level of p<0.05. For visualisation: anatomic left is on the right side of the image. MTR = magnetisation transfer ratio, MTsat = magnetisation transfer saturation, R1app = approximation of longitudinal relaxation rate, TFCE = family-wise error correction, FWE = threshold-free cluster enhancement.

3.3 Correlation between MTI metrics, T1w/T2w ratio and FA

We performed both voxel-wise (Figure 5) and tract-wise correlations (Figure 6) of T1w/T2w ratio and FA with the MTI-derived metrics. At the voxel-wise level (Figure 5), T1w/T2w ratio seems to have moderate positive correlations with MTsat (r = 0.462) and MTR (r = 0.410) and a weak positive correlation with R1app (r = 0.208); on the other hand, FA only has weak positive correlation with MTR (r = 0.258) and very weak correlations with MTsat (r = 0.161) and R1app (r = 0.114). However, these correlation trends are different at the tract level (Figure 6; Supplementary Table 2) where FA shows strong positive correlation with MTsat (mean r = 0.646) and moderate correlations with MTR (mean r = 0.512) and R1app (mean r = 0.422). However, T1w/T2w ratio shows much weaker correlations (mean r = 0.257 with MTsat, mean r = 0.254 with MTR, and mean r = 0.095 with R1app).

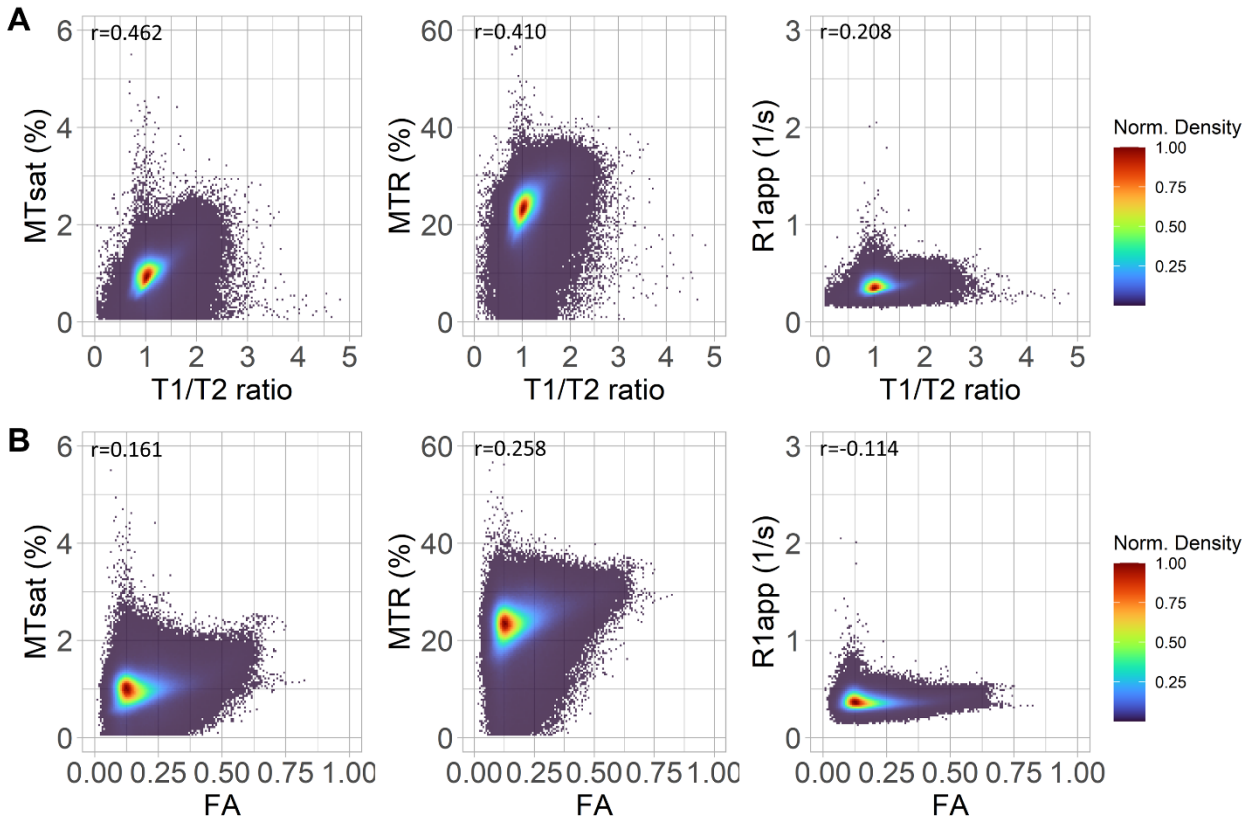

Figure 5: Two dimensional normalised density plots show the (binned voxelwise) relationship between: (A) T1w/T2w ratio and the three measures derived from magnetisation transfer imaging in white matter, and (B) FA and the three measures derived from magnetisation transfer imaging in white matter. Correlation coefficients presented are the repeated measures correlation calculated using rmcorr, with study participant as the repeated measure.

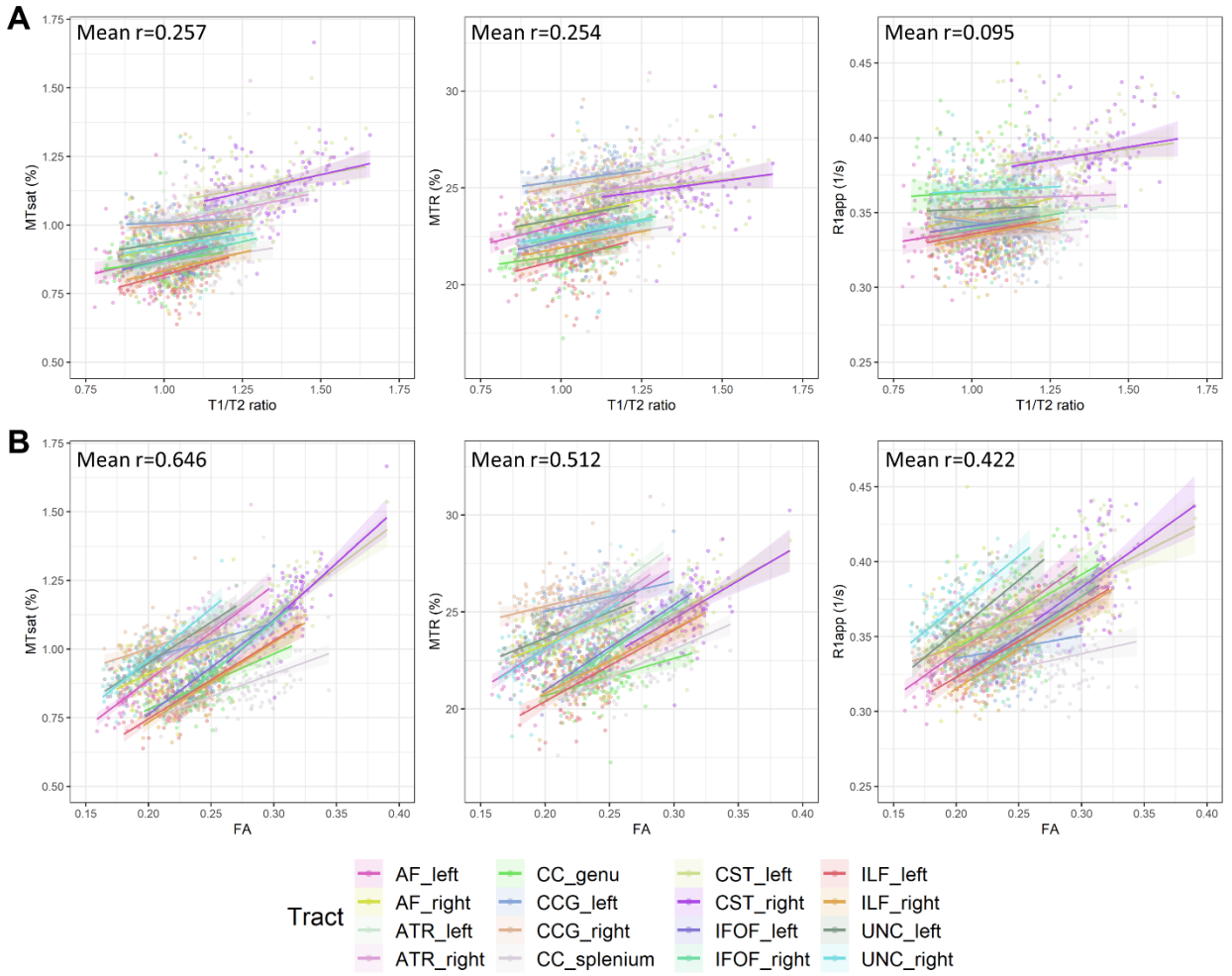

Figure 6: White matter tract-wise correlations between: (A) T1w/T2w ratio and the three measures derived from magnetisation transfer imaging, and (B) FA and the three measures derived from magnetisation transfer imaging. The average Pearson's correlation coefficient for the relationships between the tracts was calculated by first transforming the Pearson's r values to Fisher's Z, taking the average, and then back-transforming the value to Pearson's correlation coefficient.

4 Discussion

In this work, we used MTI to characterise myelination in the neonatal brain in association with age at scan and preterm birth. For the first time, MTsat was applied in the neonatal population. Across the WM, we found positive correlations between GA at scan and all MTI metrics. Preterm birth was associated with decreased R1app across the brain, increased MTR in central WM regions, and, to a lesser extent, decreased MTsat in the genu and splenium of the corpus callosum. T1w/T2w ratio had moderate positive correlations with MTR and MTsat at voxel level, but weaker within major WM tracts, whilst the opposite was observed for FA. This study contributes to the understanding of WM dysmaturation in preterm infants and how commonly used WM integrity measures relate to those more specific to myelin.

During the last trimester of pregnancy, cellular and axonal density, and the degree of axonal alignment all increase while water content decreases. In parallel, myelination events begin, resulting in increased (myelin-related) macromolecules in the brain (Dubois et al., 2014). These processes can result both in increased MTR as well as increased R1 (Grotheer et al., 2022; Nossin-Manor et al., 2015; Yeatman et al., 2014). Indeed, previous work has demonstrated that MTR is reflective of myelin content via histological analysis (Mancini et al., 2020; Schmierer et al., 2004). In the adult white matter, R1 is primarily driven by myelin content (Stüber et al., 2014), however, it is also affected by cellular density as well as by iron, calcium content, axon size and count, and free water content, which may have stronger contributions in the infant brain (Grotheer et al., 2022; Harkins et al., 2016).

Both MTsat and MTR values observed in this study are remarkably lower than previously observed in adult populations (York et al., 2022b). Average MTsat and MTR values in the WM of healthy adults are around 3.7% and 54.5%, respectively (York et al., 2022b), whilst in this neonatal sample, the range of average MTsat and MTR values in the major WM tracts are 0.8–1.18% and 21.5–26.0%, respectively. These values are even lower than those observed in the WM lesions of multiple sclerosis patients (York et al., 2022b). This is likely to reflect lower myelin density in the neonatal compared to the adult brain. However, it also raises the question to what extent MTsat and MTR values in the neonatal brain are influenced by myelin density as compared with other biological processes. It is important to note that MTR is highly protocol dependent, making comparison of values across different studies difficult; the current study applied a MT protocol similar to the one used previously in the multiple sclerosis study (York et al., 2022b). Nevertheless, MTR values in a similar range (20–30%) have been reported previously in preterm neonates at TEA (Nossin-Manor et al., 2013). Likewise, R1app values in the WM tracts in current study (0.33–0.41 s^{-1}) are similar to those R1 (=1/T1) values reported previously in the WM of preterm infants scanned between 38–43 weeks (0.34–0.44 s^{-1} (Schneider et al., 2016)), but slightly lower to the R1 values in WM bundles of new-born term infants (0.42–0.55 s^{-1} (Grotheer et al., 2022)). Similarly to Grotheer et al. (2022), we observed highest myelination (as measured by MTsat and R1app) in the corticospinal tracts, though the ranking of other tracts varies, which may be due to the differences in the infant populations studied.

We observed strong positive correlations between GA at scan and MTR across the WM, whilst the positive correlation between GA at scan and R1app was weaker and less widely distributed. These results are in line with previous studies showing higher MTR values in WM fibres with increasing age at scan during the neonatal period in preterm infants (Nossin-Manor et al., 2015, 2013) and studies showing positive correlations between postnatal age at scan and R1 over the first six months of life (Grotheer et al., 2022) as well as decrease of T1 (= 1/R1) from preterm birth up to TEA (Schneider et al., 2016). We further report strong positive correlations between GA at scan and MTsat. Taken together, these data suggest the

technique is capturing the progression in myelin density that is known to take place during the window period of data acquisition used in this study.

We observed that preterm infants have significantly lower R1app values in most of the WM compared with term infants, suggesting lower cellular and myelin density as well as lower iron, calcium content, and axonal count and size. MTsat values were lower in the preterm brain, but this was mostly limited to the genu and splenium of the corpus callosum, reflecting lower myelination in these regions compared to term-born controls, though the effect sizes were much smaller to those found for R1app. Interestingly, we found higher MTR in preterm WM than term WM, which may appear counter-intuitive. However, it is important to remember that MTR is susceptible to T1 relaxation effects (Helms et al., 2008b) and these results can be explained through the equations linking the three MTI metrics (see section 2.3 in Material and methods). For example, in the genu and splenium of the corpus callosum, term infants have both higher MTsat and R1app, resulting in no difference between the groups observed for MTR. In contrast, in the corticospinal tract, MTsat values do not differ between term and preterm infants, whilst R1app is higher in term infants; as a result, we observe lower MTR values in the term compared to preterm brain, suggesting that the higher R1 alone is driving the lower MTR values seen in term infants. These results emphasise previous observations that caution is required when interpreting MTR data; as discussed above, because of the sensitivity of R1 to a number of biological processes, the effects of preterm birth observed for MTR may not solely be driven by myelin density.

The final aim of this study was to investigate the relationship between myelin-sensitive MTI metrics and commonly used neuroimaging markers of WM dysmaturation/integrity – T1w/T2w ratio and FA. Previously, weak positive correlations have been reported between T1w/T2w ratio and MTsat (r=0.28 (Saccenti et al., 2020)) and strong correlations between T1w/T2w ratio and MTR (r=0.63 (Pareto et al., 2020)) in normal appearing WM in patients with multiple sclerosis. However, these relationships have not been studied in the neonatal brain. We observed moderate positive correlations between T1w/T2w ratio and MTR as well as MTsat in the WM at the voxel-level and weak positive correlations at tract-level. When investigating the correlations with FA, there was the opposite phenomenon as the one observed with T1w/T2w ratio: the average tract correlations within WM tracts are higher than the voxel-wise correlations. These results could potentially reflect different patterns of myelination across the brain. The general pattern of myelination relies on a caudo-rostral gradient, a progression from the brain centre to the periphery, in sensory and motor pathways before associative pathways (Dubois et al., 2021). This is reflected by our findings of correlations with differing magnitude between MTI metrics, and T1w/T2w ratio and FA across the WM tracts. FA is well-known to be affected by multiple factors based on the water content and geometry of the tracts (Figley et al., 2022), especially in crossing fibres areas, which represent around 90% of the brain (Jeurissen et al., 2013). This effect is less pronounced within the major WM tracts, where the geometry is simpler and the fibres are

better/tightly aligned (Figley et al., 2022). This could explain why, on average, the correlation of FA with the MTI metrics is larger in the specific tracts compared to the whole WM voxel-wise approach. This finding may suggest that within major WM tracts, myelin could have a significant contribution to FA. On the other hand, the relatively high positive correlations of the T1w/T2w ratio with the MTI metrics at the whole WM level are highly reduced when looking at the tract level. This suggests that anatomical specificity is important in understanding the contribution of myelin to commonly used measures of WM integrity.

This study is the first to report MTsat values in a sample of neonates comprised of term-born controls and preterm infants without major parenchymal lesions. A multimodal acquisition protocol enabled co-registration of the MT images to diffusion space for delineation of major white matter tracts. A limitation of the study is the large voxel size for the MTI (2 mm^3), but this was required to optimise acquisition parameters to achieve shorter acquisition times. Neonatal MT images are challenging to align to other modalities due to the low contrast between tissue characteristics of the neonatal brain (Dubois et al., 2021); to overcome this limitation, the T1w acquired during the MTI acquisition was co-registered to the T1w structural image, and this transformation was used as a bridge to move the maps from one space to another.

5 Conclusions

This study provides a new characterisation of the neonatal brain using MTI, and demonstrates the utility of the technique for studying disorders of myelination in early life. All MTI metrics (MTR, MTsat and R1app) increase with GA at scan. In term compared with preterm infants, MTsat and R1app are higher while MTR is lower. This could suggest confounding effects of R1 in MTR values and cautions the use of MTR to measure myelin density; MTsat may be a more reliable biomarker of myelin in the neonatal brain. In addition, by correlating MTI metrics with common WM integrity biomarkers, FA and the T1w/T2w ratio, we observed interesting opposing trends at voxel- and tract-level, which emphasises the necessity to incorporate anatomical information when interpreting the contribution of myelin to non-specific imaging metrics in early life studies.

6 CRediT authorship statement

Manuel Blesa Cábez: Conceptualization, Methodology, Software, Formal analysis, Data Curation, Writing - Original Draft, Visualization; **Kadi Vaher**: Conceptualization, Methodology, Formal analysis, Investigation, Data Curation, Writing - Original Draft, Visualization; **Elizabeth N. York**: Formal analysis, Software, Writing - Review & Editing; **Paola Galdi**: Formal analysis, Writing - Review & Editing; **Gemma Sullivan**: Investigation, Data Curation; **David Q. Stoye**: Investigation, Data Curation, Writing - Review & Editing; **Jill Hall**: Data Curation, Project administration; **Amy E. Corrigan**: Investigation, Data Curation; **Alan J. Quigley**: Investigation; **Adam D. Waldman**: Writing - Review & Editing; **Mark E. Bastin**: Methodology, Software, Resources, Writing - Review & Editing; **Michael J.**

Thrippleton: Methodology, Software, Resources, Writing - Review & Editing; **James P. Boardman**: Conceptualization, Methodology, Writing - Original Draft, Supervision, Funding acquisition.

7 Funding

This work was supported by Theirworld (www.theirworld.org) and was undertaken in the MRC Centre for Reproductive Health, which is funded by MRC Centre Grant (MRC G1002033). KV is funded by the Wellcome Translational Neuroscience PhD Programme at the University of Edinburgh (108890/Z/15/Z). PG is partly supported by the Wellcome-University of Edinburgh ISSF3 (IS3-R1.1320/21). MJT is supported by NHS Lothian Research and Development Office. ENY was supported by a Chief Scientist Office SPRINT MND/MS Studentship (MMPP/01) and funding from the Anne Rowling Regenerative Neurology Clinic, Edinburgh, United Kingdom (UK).

8 Acknowledgments

This research was funded in whole, or in part, by the Wellcome. For the purpose of open access, the author has applied a CC BY public copyright licence to any Author Accepted Manuscript version arising from this submission. We are grateful to the families who consented to take part in the study. Neonatal participants were scanned in the University of Edinburgh Imaging Research MRI Facility at the Royal Infirmary of Edinburgh which was established with funding from The Wellcome Trust, Dunhill Medical Trust, Edinburgh and Lothians Research Foundation, Theirworld, The Muir Maxwell Trust and many other sources. We are thankful to all the University's imaging research staff for providing the infant scanning.

9 References

Andersson, J.L.R., Graham, M.S., Drobnjak, I., Zhang, H., Filippini, N., Bastiani, M., 2017. Towards a comprehensive framework for movement and distortion correction of diffusion MR images: Within volume movement. Neuroimage 152, 450–466. https://doi.org/10.1016/j.neuroimage.2017.02.085

Andersson, J.L.R., Graham, M.S., Zsoldos, E., Sotiropoulos, S.N., 2016. Incorporating outlier detection and replacement into a non-parametric framework for movement and distortion correction of diffusion MR images. Neuroimage 141, 556–572. https://doi.org/10.1016/j.neuroimage.2016.06.058

Andersson, J.L.R., Skare, S., Ashburner, J., 2003. How to correct susceptibility distortions in spin-echo echo-planar images: Application to diffusion tensor imaging. Neuroimage 20, 870–888. https://doi.org/10.1016/S1053-8119(03)00336-7

Andersson, J.L.R., Sotiropoulos, S.N., 2016. An integrated approach to correction for off-resonance effects and subject movement in diffusion MR imaging. Neuroimage 125, 1063–1078. https://doi.org/10.1016/j.neuroimage.2015.10.019

Arshad, M., Stanley, J.A., Raz, N., 2017. Test–retest reliability and concurrent validity of in vivo myelin content indices: Myelin water fraction and calibrated T1w/T2w image ratio. Hum. Brain Mapp. 38, 1780–1790. https://doi.org/10.1002/HBM.23481

Avants, B.B., Epstein, C.L., Grossman, M., Gee, J.C., 2008. Symmetric diffeomorphic image registration with cross-correlation: Evaluating automated labeling of elderly and neurodegenerative brain. Med. Image Anal. 12, 26–41. https://doi.org/10.1016/J.MEDIA.2007.06.004

Back, S.A., Volpe, J.J., 2018. Encephalopathy of Prematurity: Pathophysiology, in: Volpe's Neurology of the Newborn (Sixth Edition). Elsevier, pp. 405-424.e8. https://doi.org/10.1016/B978-0-323-42876-7.00015-6

Bakdash, J.Z., Marusich, L.R., 2017. Repeated measures correlation. Front. Psychol. 8, 456. https://doi.org/10.3389/FPSYG.2017.00456/BIBTEX

Benjamini, Y., Hochberg, Y., 1995. Controlling the False Discovery Rate: A Practical and Powerful Approach to Multiple Testing. J. R. Stat. Soc. Ser. B 57, 289–300. https://doi.org/10.1111/j.2517-6161.1995.tb02031.x

Billiards, S.S., Haynes, R.L., Folkerth, R.D., Borenstein, N.S., Trachtenberg, F.L., Rowitch, D.H., Ligon, K.L., Volpe, J.J., Kinney, H.C., 2008. Myelin Abnormalities without Oligodendrocyte Loss in Periventricular Leukomalacia. Brain Pathol. 18, 153–163. https://doi.org/10.1111/J.1750-3639.2007.00107.X

Blesa, M., Galdi, P., Sullivan, G., Wheater, E.N., Stoye, D.Q., Lamb, G.J., Quigley, A.J., Thrippleton, M.J., Bastin, M.E., Boardman, J.P., 2020. Peak Width of Skeletonized Water Diffusion MRI in the Neonatal Brain. Front. Neurol. 11, 235. https://doi.org/10.3389/fneur.2020.00235

Boardman, J.P., Counsell, S.J., 2019. Invited Review: Factors associated with atypical brain development in preterm infants: insights from magnetic resonance imaging.

Neuropathol. Appl. Neurobiol. 46, 413–421. https://doi.org/10.1111/nan.12589

Boardman, J.P., Hall, J., Thrippleton, M.J., Reynolds, R.M., Bogaert, D., Davidson, D.J., Schwarze, J., Drake, A.J., Chandran, S., Bastin, M.E., Fletcher-Watson, S., 2020. Impact of preterm birth on brain development and long-term outcome: protocol for a cohort study in Scotland. BMJ Open 10, 35854. https://doi.org/10.1136/bmjopen-2019-035854

Caruyer, E., Lenglet, C., Sapiro, G., Deriche, R., 2013. Design of multishell sampling schemes with uniform coverage in diffusion MRI. Magn. Reson. Med. 69, 1534–1540. https://doi.org/10.1002/mrm.24736

Corey, D.M., Dunlap & Michael, W.P., Burke, J.J., 1998. Averaging Correlations: Expected Values and Bias in Combined Pearson rs and Fisher's z Transformations. J. Gen. Psychol. 125, 245–261. https://doi.org/10.1080/00221309809595548

Counsell, S.J., Arichi, T., Arulkumaran, S., Rutherford, M.A., 2019. Fetal and neonatal neuroimaging, in: Handbook of Clinical Neurology. Elsevier B.V., pp. 67–103. https://doi.org/10.1016/B978-0-444-64029-1.00004-7

Dubois, J., Alison, M., Counsell, S.J., Hertz-Pannier, L., Hüppi, P.S., Benders, M.J.N.L., 2021. MRI of the Neonatal Brain: A Review of Methodological Challenges and Neuroscientific Advances. J. Magn. Reson. Imaging 53, 1318–1343. https://doi.org/10.1002/JMRI.27192

Dubois, J., Dehaene-Lambertz, G., Kulikova, S., Poupon, C., Hüppi, P.S., Hertz-Pannier, L., 2014. The early development of brain white matter: A review of imaging studies in fetuses, newborns and infants. Neuroscience 276, 48–71. https://doi.org/10.1016/J.NEUROSCIENCE.2013.12.044

Figley, C.R., Uddin, M.N., Wong, K., Kornelsen, J., Puig, J., Figley, T.D., 2022. Potential Pitfalls of Using Fractional Anisotropy, Axial Diffusivity, and Radial Diffusivity as Biomarkers of Cerebral White Matter Microstructure. Front. Neurosci. 15, 1855. https://doi.org/10.3389/FNINS.2021.799576/BIBTEX

Fitzgibbon, S.P., Harrison, S.J., Jenkinson, M., Baxter, L., Robinson, E.C., Bastiani, M., Bozek, J., Karolis, V., Cordero Grande, L., Price, A.N., Hughes, E., Makropoulos, A., Passerat-Palmbach, J., Schuh, A., Gao, J., Farahibozorg, S.R., O'Muircheartaigh, J., Ciarrusta, J., O'Keeffe, C., Brandon, J., Arichi, T., Rueckert, D., Hajnal, J. V., Edwards, A.D., Smith, S.M., Duff, E., Andersson, J., 2020. The developing Human Connectome Project (dHCP) automated resting-state functional processing framework for newborn infants. Neuroimage 223, 117303. https://doi.org/10.1016/J.NEUROIMAGE.2020.117303

Glasser, M.F., van Essen, D.C., 2011. Mapping human cortical areas in vivo based on myelin content as revealed by T1- and T2-weighted MRI. J. Neurosci. 31, 11597–11616. https://doi.org/10.1523/JNEUROSCI.2180-11.2011

Greve, D.N., Fischl, B., 2009. Accurate and robust brain image alignment using boundary-based registration. Neuroimage 48, 63–72. https://doi.org/10.1016/J.NEUROIMAGE.2009.06.060

Grotheer, M., Rosenke, M., Wu, H., Kular, H., Querdasi, F.R., Natu, V.S., Yeatman, J.D., Grill-Spector, K., 2022. White matter myelination during early infancy is linked to spatial

gradients and myelin content at birth. Nat. Commun. 13, 997. https://doi.org/10.1038/s41467-022-28326-4

Harkins, K.D., Xu, J., Dula, A.N., Li, K., Valentine, W.M., Gochberg, D.F., Gore, J.C., Does, M.D., 2016. The microstructural correlates of T1 in white matter. Magn. Reson. Med. 75, 1341–1345. https://doi.org/10.1002/MRM.25709

Helms, G., Dathe, H., Dechent, P., 2010a. Modeling the influence of TR and excitation flip angle on the magnetization transfer ratio (MTR) in human brain obtained from 3D spoiled gradient echo MRI. Magn. Reson. Med. 64, 177–185. https://doi.org/10.1002/MRM.22379

Helms, G., Dathe, H., Dechent, P., 2010b. Erratum to Helms, Dathe, and Dechent. Quantitative FLASH MRI at 3 tesla using a rational approximation of the ernst equation. Magn Reson Med 2008;59:667-672. Magn. Reson. Med. 63, 1136. https://doi.org/10.1002/mrm.22293

Helms, G., Dathe, H., Dechent, P., 2008a. Quantitative FLASH MRI at 3T using a rational approximation of the Ernst equation. Magn. Reson. Med. 59, 667–672. https://doi.org/10.1002/MRM.21542

Helms, G., Dathe, H., Kallenberg, K., Dechent, P., 2008b. High-resolution maps of magnetization transfer with inherent correction for RF inhomogeneity and T1 relaxation obtained from 3D FLASH MRI. Magn. Reson. Med. 60, 1396–1407. https://doi.org/10.1002/mrm.21732

Helms, G., Hagberg, G.E., 2009. In vivo quantification of the bound pool T1 in human white matter using the binary spin–bath model of progressive magnetization transfer saturation. Phys. Med. Biol. 54, N529. https://doi.org/10.1088/0031-9155/54/23/N01

Jeurissen, B., Leemans, A., Tournier, J.D., Jones, D.K., Sijbers, J., 2013. Investigating the prevalence of complex fiber configurations in white matter tissue with diffusion magnetic resonance imaging. Hum. Brain Mapp. 34, 2747–2766. https://doi.org/10.1002/HBM.22099

Johnson, S., Marlow, N., 2017. Early and long-term outcome of infants born extremely preterm. Arch Dis Child 102, 97–102. https://doi.org/10.1136/archdischild-2015-309581

Makropoulos, A., Gousias, I.S., Ledig, C., Aljabar, P., Serag, A., Hajnal, J. V., Edwards, A.D., Counsell, S.J., Rueckert, D., 2014. Automatic whole brain MRI segmentation of the developing neonatal brain. IEEE Trans. Med. Imaging 33, 1818–1831. https://doi.org/10.1109/TMI.2014.2322280

Makropoulos, A., Robinson, E.C., Schuh, A., Wright, R., Fitzgibbon, S., Bozek, J., Counsell, S.J., Steinweg, J., Vecchiato, K., Passerat-Palmbach, J., Lenz, G., Mortari, F., Tenev, T., Duff, E.P., Bastiani, M., Cordero-Grande, L., Hughes, E., Tusor, N., Tournier, J.D., Hutter, J., Price, A.N., Teixeira, R.P.A.G., Murgasova, M., Victor, S., Kelly, C., Rutherford, M.A., Smith, S.M., Edwards, A.D., Hajnal, J. V., Jenkinson, M., Rueckert, D., 2018. The developing human connectome project: A minimal processing pipeline for neonatal cortical surface reconstruction. Neuroimage 173, 88–112.

https://doi.org/10.1016/j.neuroimage.2018.01.054

Mancini, M., Karakuzu, A., Cohen-Adad, J., Cercignani, M., Nichols, T.E., Stikov, N., 2020. An interactive meta-analysis of MRI biomarkers of Myelin. Elife 9, e61523. https://doi.org/10.7554/eLife.61523

Nosarti, C., Reichenberg, A., Murray, R.M., Cnattingius, S., Lambe, M.P., Yin, L., MacCabe, J., Rifkin, L., Hultman, C.M., 2012. Preterm birth and psychiatric disorders in young adult life. Arch. Gen. Psychiatry 69, e1-8. https://doi.org/10.1001/archgenpsychiatry.2011.1374

Nossin-Manor, R., Card, D., Morris, D., Noormohamed, S., Shroff, M.M., Whyte, H.E., Taylor, M.J., Sled, J.G., 2013. Quantitative MRI in the very preterm brain: Assessing tissue organization and myelination using magnetization transfer, diffusion tensor and T1 imaging. Neuroimage 64, 505–516. https://doi.org/10.1016/j.neuroimage.2012.08.086

Nossin-Manor, R., Card, D., Raybaud, C., Taylor, M.J., Sled, J.G., 2015. Cerebral maturation in the early preterm period-A magnetization transfer and diffusion tensor imaging study using voxel-based analysis. Neuroimage 112, 30–42. https://doi.org/10.1016/j.neuroimage.2015.02.051

Nossin-Manor, R., Chung, A.D., Whyte, H.E.A., Shroff, M.M., Taylor, M.J., Sled, J.G., 2012. Deep gray matter maturation in very preterm neonates: Regional variations and pathology-related age-dependent changes in magnetization transfer ratio. Radiology 263, 510–517. https://doi.org/10.1148/radiol.12110367

ParaView Developers, 2020. ParaView User's Guide — ParaView Documentation.

Pareto, D., Garcia-Vidal, A., Alberich, M., Auger, C., Montalban, X., Tintoré, M., Sastre-Garriga, J., Rovira, 2020. Ratio of T1-Weighted to T2-Weighted Signal Intensity as a Measure of Tissue Integrity: Comparison with Magnetization Transfer Ratio in Patients with Multiple Sclerosis. Am. J. Neuroradiol. 41, 461–463. https://doi.org/10.3174/AJNR.A6481

Pecheva, D., Kelly, C., Kimpton, J., Bonthrone, A., Batalle, D., Zhang, H., Counsell, S.J., 2018. Recent advances in diffusion neuroimaging: applications in the developing preterm brain. F1000Research 7, 1326. https://doi.org/10.12688/f1000research.15073.1

R Core Team, 2022. R: A language and environment for statistical computing. R Foundation for Statistical Computing [WWW Document]. URL https://www.r-project.org/

Saccenti, L., Hagiwara, A., Andica, C., Yokoyama, K., Fujita, S., Kato, S., Maekawa, T., Kamagata, K., Le Berre, A., Hori, M., Wada, A., Tateishi, U., Hattori, N., Aoki, S., 2020. Myelin Measurement Using Quantitative Magnetic Resonance Imaging: A Correlation Study Comparing Various Imaging Techniques in Patients with Multiple Sclerosis. Cells 2020, Vol. 9, Page 393 9, 393. https://doi.org/10.3390/CELLS9020393

Samson, R.S., Wheeler-Kingshott, C.A.M., Symms, M.R., Tozer, D.J., Tofts, P.S., 2006. A simple correction for B1 field errors in magnetization transfer ratio measurements. Magn. Reson. Imaging 24, 255–263. https://doi.org/10.1016/J.MRI.2005.10.025

Schmierer, K., Scaravilli, F., Altmann, D.R., Barker, G.J., Miller, D.H., 2004. Magnetization transfer ratio and myelin in postmortem multiple sclerosis brain. Ann. Neurol. 56, 407–415. https://doi.org/10.1002/ANA.20202

Schneider, J., Kober, T., Bickle Graz, M., Meuli, R., Hüppi, P.S., Hagmann, P., Truttmann, A.C., 2016. Evolution of T1 Relaxation, ADC, and Fractional Anisotropy during Early Brain Maturation: A Serial Imaging Study on Preterm Infants. Am. J. Neuroradiol. 37, 155–162. https://doi.org/10.3174/AJNR.A4510

Schuh, A., Makropoulos, A., Robinson, E.C., Cordero-Grande, L., Hughes, E., Hutter, J., Price, A.N., Murgasova, M., Teixeira, R.P.A.G., Tusor, N., Steinweg, J.K., Victor, S., Rutherford, M.A., Hajnal, J. V., Edwards, A.D., Rueckert, D., 2018. Unbiased construction of a temporally consistent morphological atlas of neonatal brain development. bioRxiv 251512. https://doi.org/10.1101/251512

Sled, J.G., 2018. Modelling and interpretation of magnetization transfer imaging in the brain. Neuroimage 182, 128–135. https://doi.org/10.1016/J.NEUROIMAGE.2017.11.065

Smith, S.M., Jenkinson, M., Johansen-Berg, H., Rueckert, D., Nichols, T.E., Mackay, C.E., Watkins, K.E., Ciccarelli, O., Cader, M.Z., Matthews, P.M., Behrens, T.E.J., 2006. Tract-based spatial statistics: Voxelwise analysis of multi-subject diffusion data. Neuroimage 31, 1487–1505. https://doi.org/10.1016/j.neuroimage.2006.02.024

Smith, S.M., Jenkinson, M., Woolrich, M.W., Beckmann, C.F., Behrens, T.E.J., Johansen-Berg, H., Bannister, P.R., De Luca, M., Drobnjak, I., Flitney, D.E., Niazy, R.K., Saunders, J., Vickers, J., Zhang, Y., De Stefano, N., Brady, J.M., Matthews, P.M., 2004. Advances in functional and structural MR image analysis and implementation as FSL. Neuroimage 23, S208–S219. https://doi.org/10.1016/j.neuroimage.2004.07.051

Smith, S.M., Nichols, T.E., 2009. Threshold-free cluster enhancement: Addressing problems of smoothing, threshold dependence and localisation in cluster inference. Neuroimage 44, 83–98. https://doi.org/10.1016/j.neuroimage.2008.03.061

Soun, J.E., Liu, M.Z., Cauley, K.A., Grinband, J., 2017. Evaluation of neonatal brain myelination using the T1- and T2-weighted MRI ratio. J. Magn. Reson. Imaging 46, 690–696. https://doi.org/10.1002/JMRI.25570

Stüber, C., Morawski, M., Schäfer, A., Labadie, C., Wähnert, M., Leuze, C., Streicher, M., Barapatre, N., Reimann, K., Geyer, S., Spemann, D., Turner, R., 2014. Myelin and iron concentration in the human brain: A quantitative study of MRI contrast. Neuroimage 93, 95–106. https://doi.org/10.1016/J.NEUROIMAGE.2014.02.026

Thompson, D.K., Yang, J.Y.M., Chen, J., Kelly, C.E., Adamson, C.L., Alexander, B., Gilchrist, C., Matthews, L.G., Lee, K.J., Hunt, R.W., Cheong, J.L.Y., Spencer-Smith, M., Neil, J.J., Seal, M.L., Inder, T.E., Doyle, L.W., Anderson, P.J., 2022. Brain White Matter Development Over the First 13 Years in Very Preterm and Typically Developing Children Based on the T1-w/T2-w Ratio. Neurology 98, e924–e937. https://doi.org/10.1212/WNL.0000000000013250

Tournier, J.D., Smith, R., Raffelt, D., Tabbara, R., Dhollander, T., Pietsch, M., Christiaens, D., Jeurissen, B., Yeh, C.H., Connelly, A., 2019. MRtrix3: A fast, flexible and open software

framework for medical image processing and visualisation. Neuroimage 202, 116137. https://doi.org/10.1016/J.NEUROIMAGE.2019.116137

Tustison, N.J., Avants, B.B., Cook, P.A., Zheng, Y., Egan, A., Yushkevich, P.A., Gee, J.C., 2010. N4ITK: Improved N3 bias correction. IEEE Trans. Med. Imaging 29, 1310–1320. https://doi.org/10.1109/TMI.2010.2046908

Uddin, M.N., Figley, T.D., Marrie, R.A., Figley, C.R., 2018. Can T1w/T2w ratio be used as a myelin-specific measure in subcortical structures? Comparisons between FSE-based T1w/T2w ratios, GRASE-based T1w/T2w ratios and multi-echo GRASE-based myelin water fractions. NMR Biomed. 31, e3868. https://doi.org/10.1002/NBM.3868

Vaher, K., Galdi, P., Blesa Cabez, M., Sullivan, G., Stoye, D.Q., Quigley, A.J., Thrippleton, M.J., Bogaert, D., Bastin, M.E., Cox, S.R., Boardman, J.P., 2022. General factors of white matter microstructure from DTI and NODDI in the developing brain. Neuroimage 254, 119169. https://doi.org/10.1016/J.NEUROIMAGE.2022.119169

van der Weijden, C.W.J., García, D.V., Borra, R.J.H., Thurner, P., Meilof, J.F., van Laar, P.-J., Dierckx, P.R.A.J.O., Gutmann, I.W., de Vries, E.F.J., 2020. Myelin quantification with MRI: A systematic review of accuracy and reproducibility. Neuroimage 117561. https://doi.org/10.1016/j.neuroimage.2020.117561

Vandewouw, M.M., Young, J.M., Shroff, M.M., Taylor, M.J., Sled, J.G., 2019. Altered myelin maturation in four year old children born very preterm. NeuroImage Clin. 21, 101635. https://doi.org/10.1016/j.nicl.2018.101635

Veraart, J., Novikov, D.S., Christiaens, D., Ades-aron, B., Sijbers, J., Fieremans, E., 2016. Denoising of diffusion MRI using random matrix theory. Neuroimage 142, 394–406. https://doi.org/10.1016/j.neuroimage.2016.08.016

Volpe, J.J., 2019. Dysmaturation of Premature Brain: Importance, Cellular Mechanisms, and Potential Interventions. Pediatr. Neurol. 95, 42–66. https://doi.org/10.1016/J.PEDIATRNEUROL.2019.02.016

Volpe, J.J., Kinney, H.C., Jensen, F.E., Rosenberg, P.A., 2011. The developing oligodendrocyte: key cellular target in brain injury in the premature infant. Int. J. Dev. Neurosci. 29, 423. https://doi.org/10.1016/J.IJDEVNEU.2011.02.012

Winkler, A.M., Ridgway, G.R., Webster, M.A., Smith, S.M., Nichols, T.E., 2014. Permutation inference for the general linear model. Neuroimage 92, 381–397. https://doi.org/10.1016/j.neuroimage.2014.01.060

Wolke, D., Johnson, S., Mendonça, M., 2019. The Life Course Consequences of Very Preterm Birth. Annu. Rev. Dev. Psychol. 1, 69–92. https://doi.org/10.1146/ANNUREV-DEVPSYCH-121318-084804

Yeatman, J.D., Wandell, B.A., Mezer, A.A., 2014. Lifespan maturation and degeneration of human brain white matter. Nat. Commun. 2014 51 5, 1–12. https://doi.org/10.1038/ncomms5932

York, E.N., Meijboom, R., Kampaite, A., Valdes Hernandez, M., Thrippleton, M.J., Waldman, A.D., 2022a. Magnetisation transfer saturation (MTsat) and MTR: relationship with T1

recovery in multiple sclerosis and healthy brain, in: ISMRM.

York, E.N., Meijboom, R., Thrippleton, M.J., Bastin, M.E., Kampaite, A., White, N., Chandran, S., Waldman, A.D., 2022b. Longitudinal microstructural MRI markers of demyelination and neurodegeneration in early relapsing-remitting multiple sclerosis: Magnetisation transfer, water diffusion and g-ratio. NeuroImage Clin. 36, 103228. https://doi.org/10.1016/J.NICL.2022.103228

York, E.N., Thrippleton, M.J., Meijboom, R., Hunt, D.P.J., Waldman, A.D., 2022c. Quantitative magnetization transfer imaging in relapsing-remitting multiple sclerosis: a systematic review and meta-analysis. Brain Commun. 4. https://doi.org/10.1093/BRAINCOMMS/FCAC088

York, E.N., Thrippleton, M.J., Waldman, A., 2020. Magnetisation transfer saturation (MTsat) processing. https://doi.org/10.7488/DS/2965

Zheng, Y., Wang, X., Zhao, X., 2016. Magnetization transfer and amide proton transfer MRI of neonatal brain development. Biomed Res. Int. 2016. https://doi.org/10.1155/2016/3052723